Biosensors and Bioelectronics 31 (2012) 17–25

Contents lists available at SciVerse ScienceDirect

Biosensors and Bioelectronics

journal homepage: www.elsevier.com/locate/bios

Tunable pores for measuring concentrations of synthetic and biological nanoparticle dispersions

G. Seth Roberts[a], Sam Yu[a], Qinglu Zeng[b], Leslie C.L. Chan[c], Will Anderson[a], Aaron H. Colby[d], Mark W. Grinstaff[d], Steven Reid[c], Robert Vogel[e,*]

[a] Izon Science Ltd, PO Box 39168, Harewood, Christchurch 8545, New Zealand
[b] Civil and Environmental Engineering, MIT 48-424, 15 Vassar Street, Cambridge, MA 02139, USA
[c] Australian Institute for Bioengineering and Nanotechnology, University of Queensland, St Lucia, Queensland 4072, Australia
[d] Departments of Biomedical Engineering and Chemistry, Boston University, Boston, MA, 02215, USA
[e] Centre for Biophotonics and Laser Science, School of Mathematics and Physics, University of Queensland, St Lucia, Queensland 4072, Australia

ARTICLE INFO

Article history:
Received 19 August 2011
Accepted 19 September 2011
Available online 5 October 2011

Keywords:
Concentration
Nanoparticles
Resistive pulse sensing
Coulter counter
Nanopores
Actuation

ABSTRACT

Scanning ion occlusion sensing (SIOS), a technique that uses a tunable pore to detect the passage of individual nano-scale objects, is applied here for the rapid, accurate and direct measurement of synthetic and biological nanoparticle concentrations. SIOS is able to characterize smaller particles than other direct count techniques such as flow cytometry or Coulter counters, and the direct count avoids approximations such as those necessary for turbidity measurements. Measurements in a model system of 210–710 nm diameter polystyrene particles demonstrate that the event frequency scales linearly with applied pressure and concentration, and that measured concentrations are independent of particle type and size. Both an external-calibration and a calibration-free measurement method are demonstrated. SIOS is then applied to measure concentrations of Baculovirus occlusion bodies, with a diameter of ~1 μm, and the marine photosynthetic cyanobacterium *Prochlorococcus*, with a diameter of ~600 nm. The determined concentrations agree well with results from counting with microscopy (a 17% difference between the mean concentrations) and flow cytometry (6% difference between the mean concentrations), respectively.

1. Introduction

Synthetic and biological nanoparticles have found increasing use in high-profile applications such as electronic ink (Oh et al., 2009; Park et al., 2006), drug delivery (Brannon-Peppas and Blanchette, 2004; Jin and Ye, 2007) and gene therapy (Campos and Barry, 2007; Jin and Ye, 2007), with nanoparticles employed as vectors in therapies for cancer (Colson et al., 2011; Cuenca et al., 2006; Tanaka et al., 2009), blood disorders (Nienhuis, 2008) and Alzheimer's disease (Cui et al., 2005).

An accurate characterization of both size and concentration in nanoparticle systems is desirable for many applications, and can be critical in applications such as medical therapies. The particle size affects the vectors' efficacy for delivery and dictates the amount of therapeutic agent that can be loaded, while the particle concentration determines the overall dose. However – even in an application that depends so critically on both particle size and concentration – while considerable attention has been given to the influence of nanoparticle size and shape on therapy outcomes (Chithrani et al., 2006; Ferrari, 2008; Jiang et al., 2008), the lack of applicable, accurate techniques to measure nanoparticle concentrations has resulted in a lack of data on the effects of nanoparticle number concentration. The applied dose is typically calculated using the weight or volume fraction of a nanoparticle dispersion (Cohen-Sela et al., 2006; Cui et al., 2005; Mukherjee et al., 2007; Westedt et al., 2004), a method susceptible to errors in particle polydispersity and mass measurement. A system that gives accurate information on size and concentration could be used to better characterize particle dispersions, an outcome with beneficial implications for all nanoparticle applications.

While size data can be obtained using methods such as dynamic light scattering (Russel et al., 1992), disc centrifugation (Bondoc-Jr and Fitzpatrick, 1998), gel electrophoresis (Alberts et al., 1994) or electron microscopy (SEM or TEM), nanoparticle concentrations are more difficult to determine. Conventional techniques such as flow cytometry (Shapiro, 2003) and Coulter counters (Bayley and Martin, 2000) have a number of limitations, including the need for large sample volumes and an inability to accurately detect particles smaller than ~400 nm (Bayley and Martin, 2000; Shapiro, 2003), while weight fraction determination can only be accurate for high concentrations of monodisperse particles.

Techniques for measuring biological nanoparticle concentrations include qPCR (Ma et al., 2001), ELISA assays (Johansson et al., 1980) and UV/vis spectroscopy (Maizel et al., 1968), and while

* Corresponding author. Tel.: +61 0 404 385 636; fax: +61 0 7 3365 1242.
E-mail address: vogel@physics.uq.edu.au (R. Vogel).

0956-5663/$ – see front matter © 2011 Elsevier B.V. All rights reserved.
doi:10.1016/j.bios.2011.09.040

these methods are able to deal with small bodies, they do not directly detect particles. Larger particles can be counted directly via microscopy (Chakraborty et al., 1996), but this method is labour intensive, slow and inaccurate. Nanopore Coulter counters show great promise for the direct determination of nanoparticle concentrations, having been applied to count viruses (Deblois and Wesley, 1977) and synthetic particles from 56 to 90 nm (Deblois and Bean, 1970; Ito et al., 2004; Saleh and Sohn, 2001); Fraikin et al. (2011) describe the application of a microfluidic device and a method similar to that described here to measure the size and concentration in polydisperse synthetic nanoparticle solutions (sizes from 51 to 117 nm), as well as the size and concentration of viral particles in mouse blood plasma. However, all these devices have a limited dynamic range, due to their fixed pore/channel size.

In this paper, the application of a tunable pore device to measure particle dispersion concentrations is described. SIOS (Sowerby et al., 2007) uses a size-tunable pore manufactured in a polyurethane membrane to detect the passage of nano or micron sized particles as a drop in the ionic current measured across the pore. The flexible nature of the pore membrane means that the pore size can be optimized in real time for the experimental conditions at hand, a property that has been exploited to gate particles by size and detect DNA modification of organosilica nanoparticles (Roberts et al., 2010), and to accurately size particles ranging from 97 nm to 2 μm (Vogel et al., 2011). Pores of different size can be produced through variations in the manufacturing process, allowing the detection of particles from 50 nm to 10 μm. This wide detection range is a major advantage of SIOS over other pore-based concentration measurement techniques. Furthermore, the tunability of a single pore allows the detection of a large range of particle sizes to be optimized, a process that may require the manufacture of a new pore in fixed pore technologies. This allows the analysis of polydisperse samples, something that is difficult with fixed pore technologies. The detection and counting of individual particles combined with the ability to measure particle size also means that SIOS can be used to determine the proportion of a particle population that falls within a certain size range. A recent review of developments in nanopore technology gives a summary of previous publications on SIOS (Kozak et al., 2011).

Herein we demonstrate the first use of SIOS for the accurate, direct, rapid, in-sample measurement of quantitative nanoparticle concentrations, for ~200 nm to ~1 μm, synthetic and biological particles. Previous work using this technique (Willmott et al., 2010) demonstrated in a model system of synthetic polystyrene nanoparticles that the particle count rate scaled linearly with both applied pressure and particle concentration. We show that this behaviour agrees with theory derived from the Hagen Poiseuille equation (Tritton, 1988), and extend this work by showing that the measured particle concentration is independent of particle size and surface charge. We also show that no particle-size-dependent gating results from the use of the tunable pore. Both an external-calibration and a calibration-free method to measure the particle concentration are demonstrated. SIOS is then applied to measure concentrations in two biological samples, first for Baculovirus occlusion bodies (OBs) and then for the marine cyanobacterium *Prochlorococcus*. The results shown in this study illustrate the ability of SIOS to operate in complex biological systems, and demonstrate the wide size range of particles that can be analyzed.

2. Materials and methods

2.1. SIOS

Detailed descriptions of the device, pore manufacture and pore characteristics can be found in previously published work (Kozak et al., 2011; Roberts et al., 2010; Sowerby et al., 2007; Willmott and Moore, 2008; Willmott et al., 2010). Briefly, the pore is manufactured by mechanically puncturing a ~0.25 mm thick polyurethane membrane. This produces an approximately conically shaped pore with a size that is dependent on the puncturing process. The membrane containing this pore is then sandwiched in a fluid cell in the SIOS device and stretched onto four jaws, which provide orthogonal stretch in two dimensions in the horizontal plane. Macroscopic stretching from 0 to 10 mm applied using these jaws produces nanoscopic changes in the pore size (where macroscopic stretch is defined as the horizontal displacement of the jaws that apply stretch to the membrane). The fluid cell incorporates electrodes, which are used to apply an electric field and to monitor the current produced in the electrolyte solution contained in the fluid cell. A change in the pore size is then detected as a change in the base current level, while the passage of suspended particles through the pore is detected as a momentary drop in the measured current (a 'blockade'). A count of these blockades in a measured time gives the particle count rate.

Concentration measurements are carried out by recording the particle count rate at different applied pressures with the same applied electric field and pore size, with concentrations calculated from this data using either a calibration-free method (which uses a measurement of the pore dimensions) or a calibration performed using a reference particle suspension (as described in Section 3). The application of pressure to the sample is achieved using an external manometer, which has a range of −1.8 kPa to 1.8 kPa. While enabling the determination of particle concentrations, the application of pressure also holds advantages for low concentration samples – if the particle count frequency is too low, one can simply apply a higher pressure to increase it. The vertical orientation of the SIOS instrument means that an inherent pressure is exerted by the sample in the top half of the fluid cell. For a typical sample volume of 40 μl this pressure has a value of approximately 0.04–0.05 kPa, or only ~2.8% of the maximum pressure that can be applied using the external manometer. Since this effect is constant at all pressures, and therefore does not affect the particle count vs. pressure gradient used to calculate concentrations, it is ignored in the experiments described here.

Size calibrations are performed using a particle suspension of known size as a reference. The particle size distribution of the unknown sample is calculated using a comparison between the blockade magnitude distributions of the calibration and unknown samples (Vogel et al., 2011).

Experiments are carried out using an applied voltage of 0.3 V, and measurements are typically repeated three times. Differences in data are taken as significant if the P value is less than 0.05.

2.2. Particles and solutions

Carboxyl-modified polystyrene particles (of diameter 210 nm, 220 nm, 380 nm, 400 nm, 710 nm, 780 nm and 920 nm) were sourced from Thermofisher, Invitrogen and Polysciences. These particles will be referred to as Po210, Th220, Th380, Th400, In400, In710, Th780 and Po920. Unmodified, NIST traceable polystyrene particles (of diameter 400 nm and 500 nm) were sourced from Thermofisher. These particles will be referred to as ThNT400 and ThNT500. Carboxylated particles were used to avoid aggregation at high particle concentrations. The Baculovirus occlusion bodies studied were derived from the *Helicoverpa armigera* single-nucleocapsid nucleopolyhedrovirus (HaSNPV Strain H25EA1, an Australian isolate obtained from CSIRO Entomology, Canberra). The OBs were produced in *H. armigera* insect larvae and were purified by maceration of larvae in 0.1% SDS, filtration to remove insect debris, centrifugation of filtrate (3000 × g for 30 min), and resuspension of the OB pellet in deionized water. Axenic *Prochlorococcus*

MED4 was grown in filtered (0.22 μm filter, Whatman) Sargasso seawater-based Pro99 medium (Moore et al., 2002), and fixed with 0.5% glutaraldehyde. For SIOS experiments, the polystyrene and virus particles were suspended in buffered electrolyte consisting of 0.1 M KCl, 15 mM Tris buffer, 0.01% Triton X-100 and 3 mM EDTA, pH 8.0. For the *Prochlorococcus* concentration measurements, Pro99 medium acted as a replacement electrolyte for the Tris buffered KCl solution, for both the bacteria and the polystyrene calibration particles.

The compounds and concentrations used in the Tris buffer were originally chosen with biological applications in mind; the ion concentration gives a solution conductivity similar to that of some biological fluids, and the Tris buffer and pH were used because of their suitability for biological systems. Many experiments have shown that this buffer is also suitable for silica and polystyrene nanoparticles, as well as for DNA, streptavidin, liposomes, and other biological systems (as shown in the present manuscript, and in other publications (Roberts et al., 2010; Vogel et al., 2011; Willmott et al., 2010). The use of other buffer solutions may be necessary for different systems (for example, as shown in this manuscript for the *Prochlorococcus* concentration measurements, where a Pro99 solution was used).

2.3. Measurement of pore dimensions

The pore dimensions are determined using confocal microscopy and SEM, as described previously (Roberts et al., 2010; Vogel et al., 2011). Briefly, the pore length is determined by dyeing the membrane walls with a fluorescent solution of Rhodamine B, then imaging the pore with confocal microscopy. The small and large-side pore sizes at different macroscopic stretches are determined using SEM. The perimeter and enclosed areas of the small and large-side apertures are determined from the SEM images using Image Pro software.

3. Theoretical basis

Particle concentrations are calculated using the expression

$$J = CQ \tag{1}$$

where J is the particle count rate, C is the particle concentration and Q is the fluid flow rate (Deblois et al., 1977). Modification of the Hagen–Poiseuille equation (Eq. (A2) in Appendix A) (Tritton, 1988) to account for the near-conical geometry of the pore results in the following expression for Q:

$$Q = \frac{3\pi P}{8\eta L}\frac{b-a}{b^3-a^3}a^3b^3 \tag{2}$$

Here P is the applied pressure, η is the fluid viscosity, L is the length of the pipe, a is the radius of the small pore opening and b is the radius of the large pore opening. With the application of an end correction for slow viscous flow in a long tube and corrections for non-circular pore geometries, a full expression for the theoretical particle concentration is obtained:

$$C = J\left(\frac{3\pi P}{8\eta L_h}\frac{b_h-a_h}{b_h^3-a_h^3}a_h^3b_h^3\right)^{-1} \tag{3}$$

where L_h, a_h and b_h are the hydrodynamic pore length (Deblois et al., 1977) and hydrodynamic radii. A full description and derivation of this theory is given in Appendix A (where equation numbers have the prefix 'A'). This theory can be used to calculate particle concentrations using two different methods.

3.1. Calibration method

In Eq. (2), $Q \propto P$. Therefore from Eq. (1) a plot of particle count rate (J) vs applied pressure (P) gives a gradient proportional to C. For a pore of unknown length and diameter, the use of a calibration sample of known concentration allows the unknown concentration of a different sample to be calculated using the relation

$$C_2 = \left(\frac{g_2}{g_1}\right)C_1 \tag{4}$$

where C_1 and g_1 are, respectively, the concentration of the calibration sample and its associated gradient taken from a linear fit to the plot of measured count rate vs pressure. g_2 is the gradient associated with the sample of unknown concentration and C_2 is the unknown concentration.

3.2. Calibration-free method

The particle concentration can be calculated without the need for any external calibration standard. This is achieved by measuring the particle count rate J at a given pressure P, as well as at $P = 0$. A subtraction of the count rate at $P = 0$ from that at P gives the count rate due to applied pressure. Using this information along with the hydrodynamic pore length and radii (calculated using Eqs. (A8) and (A11) and the pore dimensions, measured as described in Section 2.3), Eq. (3) can be used to calculate the particle concentration, C.

4. Results and discussion

4.1. Proof of principle measurements in a model system

The calculation of particle concentration can be achieved using two methods. When the pore geometry is known – having been determined using microscopy (Vogel et al., 2011) – the calibration-free method as described in Section 3.2 can be used. If the pore dimensions are not known, a sample of known particle concentration can be used as an external calibration, as described in Section 3.1. In this section these calculation methods are demonstrated. This demonstration is preceded by data illustrating the sound fundamental principles upon which SIOS concentration measurements are based. Data from a typical concentration measurement shows that detection events are recorded at a constant rate and that particle aggregation does not occur, and an experiment in which particle count rates are recorded for different particle sizes with varying pore size shows that no particle-size dependent gating occurs. Further experiments show that, in agreement with theory, particle count rates scale linearly with both pressure and concentration and are independent of particle size and type.

For an accurate determination of particle concentration, it is necessary that particle aggregation and blockage of the pore do not occur. The detection of the passage of aggregates as single events could result in an underestimate of the particle concentration, while blockage of the pore impedes (or may even completely halt) the flow of particles. Fig. 1(a) shows a typical plot of particle counts against time, with an inset showing a typical (and corresponding) blockade magnitude histogram. The particle count plot shows that the passage of the detected particles is smooth and uniform with time, indicating no blockage of the pore. The single peak in the blockade magnitude histogram suggests that only single particles are detected; with the passage of aggregates we would expect additional peaks at multiples of the single particle size. These are not observed in the blockade magnitude histogram and therefore an accurate particle count is expected.

It should be noted here that in real biological samples with polydisperse particle sizes, aggregation might present problems. In such situations, some sample pre-processing may be necessary.

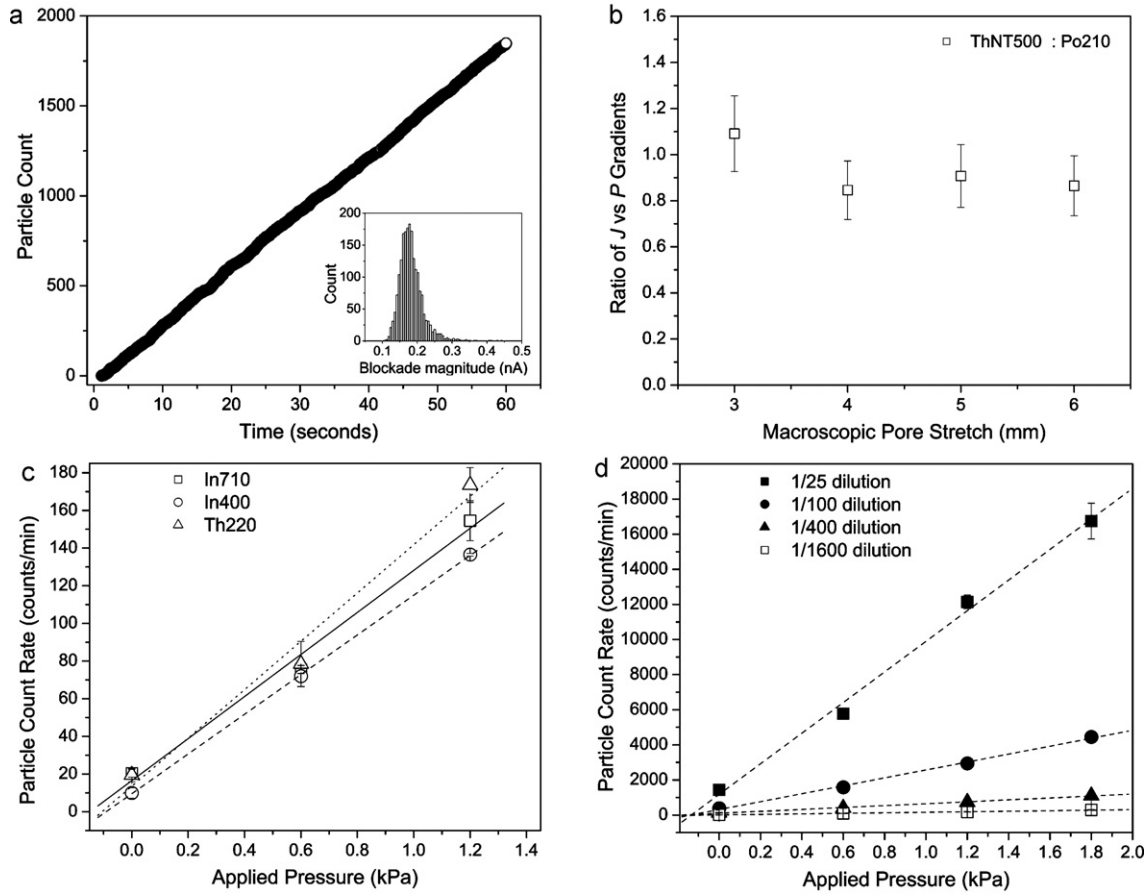

Fig. 1. (a) Typical plot of particle count against time, with inset showing the corresponding blockade magnitude histogram. (b) Plot of the ratio of the gradients from particle count rate against pressure plots for ThNT500 and Po210 particles against macroscopic pore stretch, from an experiment testing the particle size-dependent gating effects of the tunable pore. (c) Plot of particle count rate against applied pressure demonstrating the independence of the determined concentration from particle size (d) Plot of particle count rate against applied pressure for different dilutions of Th400 particles.

A simple dilution may be sufficient, but filtering steps may be required. If an aggregation-induced pore blockage does occur, in most cases it can be cleared by exploiting the tunability of the pore.

For accurate determination of particle concentration for particles of all sizes to be possible, it is necessary that a change in the pore size changes the count rates of particles of different size by the same proportion, i.e. gating of one particle size relative to another does not occur over a significant range of pore sizes. Fig. 1(b) shows data from an experiment in which the gating effects of the tunable pore were investigated. Two dispersions were prepared with different particle sizes but similar concentrations, with both Po210 and ThNT500 particles at a (manufacturer-defined) concentration of 5.0×10^9 ml^{-1} (after dilution). The particle count rate was recorded for each sample at applied pressures of 0 kPa, 0.5 kPa and 1.0 kPa at macroscopic pore stretches varying from 1 to 6 mm. The gradients from plots of particle count rate against pressure for each sample at each macroscopic stretch were then determined. Fig. 1(b) shows a plot of the ratios of these gradients (with the gradients for ThNT500 taken as a reference, so the ratio plotted is ThNT500:Po210) as a function of macroscopic pore stretch. Since the gradient is proportional to the particle concentration (see Section 3) these ratios also represent the ratios of the measured particle concentration. Fig. 1(b) shows that the ratios of the gradients remain within ±15% of unity over the range of macroscopic pore stretches shown, with no trend visible. This variation is within the random experimental error, which is also ∼±15%. At macroscopic pore stretches ≤2 mm the pore became too small for the 500 nm particles to traverse it, and hence the blockade frequency dropped to zero. These data illustrate that selective gating of larger particles occurs within 1 mm of macroscopic pore stretch, and so is effectively an on/off transition. This confirms that the tunability of the pore confers the advantage of being able to adjust the pore size to suit the size of the particles under study without compromising the ability to accurately measure the particle concentration.

The experiments described above show that none of the fundamental elements of the SIOS setup, i.e. the tunable pore and a typical particle solution, present any limitations to the accurate measurement of particle concentrations. Further experiments were conducted to investigate the validity of the theory described in Section 3 in describing the behaviour of the system. Eq. (3) predicts that the measured concentration should be independent of particle size and charge. (This independence of charge holds for the pore-sizes and significant electrolyte concentrations used in this study. For small pores and low electrolyte concentrations the charge may play a larger role (Joshi et al., 2009)). From Eqs. (1) and (2) it is also apparent that the particle count rate should scale linearly with both applied pressure and concentration. Data from experiments designed to test these hypotheses are described here.

Fig. 1(c) shows data from an experiment in which three suspensions of carboxyl-modified polystyrene particles with similar concentration but different particle size were analyzed. The three particle suspensions were diluted from the manufacturers' specified concentration into Tris buffered KCL solution to give samples with size and concentration respectively of 710 nm (In710) and 1.20×10^8 ml^{-1}, 400 nm (In400) and 1.20×10^8 ml^{-1} and 220 nm (Th220) and 1.20×10^8 ml^{-1}. The repeatability of the

Table 1
A comparison of gradient and concentration information for size-independence and count rate scaling experiments.

Experiment	Particle	Dilution	Gradient from fit	Gradient scaling factor	Manufacturer concentration	Measured concentration	% Difference
1(c)	Th220	1/14,200	128.3 ± 17.3	1.22	1.20×10^8	–	21.7
1(c)	Th400	1/2300	130.8 ± 4.3	1.24	1.22×10^8	–	24.1
1(c)	In400	1/10,000	105.4 ± 1.2	1	1.20×10^8	–	–
1(c)	In710	1/1750	111.6 ± 11.5	1.06	1.20×10^8	–	5.9
1(d)	Th400	1/25	8719.8 ± 448.9	1	1.12×10^{10}	–	–
1(d)	Th400	1/100	2243.1 ± 22.9	1/3.89	2.80×10^9	$(2.88 \pm 0.21) \times 10^9$	2.9
1(d)	Th400	1/400	542.4 ± 14.7	1/16.08	7.00×10^8	$(6.97 \pm 0.54) \times 10^8$	0.5
1(d)	Th400	1/1600	133.5 ± 6.4	1/65.32	1.75×10^8	$(1.71 \pm 0.15) \times 10^8$	2

Data corresponding to the plots shown in Fig. 1(c and d). Details are shown for the dilution of each sample, along with the gradient taken from fits to the data, the gradient scaling factors, the manufacturer-defined concentration, the measured concentration and the percentage difference between each gradient and the In400 gradient (taken as a reference) for experiment 1(c), and for experiment 1(d) the percentage difference between the manufacturer defined concentration and the measured concentration.

measurements is represented in the error bars, which show standard deviations calculated from measurements repeated in triplicate (standard deviation values were found ranging from 3% to 18% of the mean count rate at each pressure). The gradients taken from linear fits to the data are shown in Table 1. As described in Section 3.1, the calculated concentration is proportional to the gradient, and so the percentage difference in the gradients also represents the percentage difference in the calculated concentrations.

Taking the smallest gradient as a reference (from In400), the difference between this and the largest gradient (from Th220) is 21.7%. It is interesting to note that this 21.7% difference is between samples of particles from different manufacturers; the difference between the gradients of the two Invitrogen samples (400 nm and 710 nm) is only 5.9%. Th400 was also analyzed in this experiment, but the data is omitted from Fig. 1(c) (but included in Table 1) for the sake of clarity. The difference in the means of the gradients from each manufacturer (19.4%) is approximately four times the largest standard deviation for each manufacturer (4.4%), and significantly larger than the maximum error in the gradient. This ~20% error between repeated measurements is taken to be the maximum error in a SIOS concentration measurement, but these data also suggest the possibility of systematic errors in the manufacturers' determination of sample concentration (typically measured using gravimetry). Taking into account the limitations of these data, we propose that this experiment illustrates the measured concentration's independence of particle size. An additional demonstration of the independence of the concentration from particle size is given by the data from the gating experiment, shown in Fig. 1(b). As well as illustrating independence from particle size, this data also shows that measurements of the particle concentration are independent of particle charge, since the ThNT500 particles are unmodified polystyrene, with a low charge, while the Po210 particles are highly charged, carboxyl-modified polystyrene.

Fig. 1(d) shows data from an experiment in which data was collected for four different dilutions of Th400. The particles were diluted from a stock solution of concentration 2.80×10^{11} ml^{-1} (as defined by the manufacturer) with dilution factors of 25, 100, 400 and 1600. For each concentration, data was recorded at 4 pressures from 0 to 1.8 kPa. The repeatability of the measurements is shown in the error bars, which represent the standard deviation in the count rate for each set of repeated measurements. In all cases these errors are smaller than 15%. As expected from Eqs. (1) and (2) (and as shown in previous work (Willmott et al., 2010)), the particle count rate for each different concentration scales linearly with pressure, with $R^2 > 0.991$ for all linear fits. An analysis of the gradients from these linear fits for each particle concentration shows that the particle count rate also scales linearly with concentration.

Table 1 details the gradients from each of the linear fits, the scaling factor associated with each gradient, the known concentration of each sample, the determined concentrations and the percentage difference between the known and determined concentrations. The highest concentration sample (1/25 dilution, 1.12×10^{10} ml^{-1}) was taken as the calibration to determine the other concentrations and as the reference for the scaling (this sample was chosen as the calibration because of its higher count rates, and therefore greater statistical reliability). The other samples are diluted in sequence by a factor of 4, and since the gradient is proportional to the concentration we expect the gradients to be scaled by 1/4, 1/16 and 1/64. The % difference between the measured and known concentrations also represents the % difference between the measured and predicted scaling of the gradient. The largest difference observed between the measured and known concentrations (and the measured and predicted scaling factor for the gradient) is 2.9%, a value that is well within the calculated experimental errors of 7–9%. Similar experiments with polystyrene particles of size 100 nm (Willmott et al., 2010), 220 nm and 710 nm (data not shown here) gave results that agree well with the findings shown here. These results show that the particle count rate does indeed scale linearly both with pressure and with concentration. The linearity with concentration is a good indication of the lack of aggregation, since if significant aggregation were occurring at higher concentrations a deviation from linearity would be expected.

The results from these experiments agree well with the predictions of the theory in Section 3. This theory is now applied to the calculation of particle concentrations using the external calibration and calibration-free methods as described in Sections 3.1 and 3.2, and a discussion is made of the possible sources of error.

The data shown in Fig. 1(d) were taken using different dilutions of the same particle dispersion. This use of one of the dilutions as a calibration to determine the concentration of the others acts as close as is possible to a test of the external calibration method (as described in Section 3.1) using an exactly known concentration, and eliminates the effects of errors in the manufacturer-defined concentration. As shown in Table 1, the largest difference between the measured and calibration-determined gradient (and therefore concentration) is 2.9%. This result illustrates the accuracy of the external calibration method in the ideal situation of an exactly known calibration concentration. The data in Fig. 1(c) show a discrepancy between the measured gradients (and concentrations) for dispersions of ostensibly similar concentration for particles from different manufacturers, but very close agreement for dispersions of particles from the same manufacturer. This data illustrates the limitations of using a reference particle sample to calibrate for the measurement of an unknown concentration; the validity of the results depends on the accuracy of a previous concentration measurement.

In order to demonstrate the calibration-free concentration determination method, NIST traceable polystyrene particles with a diameter of 400 nm (ThNT400) were diluted from the manufacturer-specified concentration to give a concentration of 5.68×10^8 ml^{-1}. Data was taken at applied pressures of 0 kPa

and 1.0 kPa, with a macroscopic pore stretch of 3 mm. The mean measured pressure-related particle count rate, calculated from repeated measurements, was 399 min^{-1}, or 6.65 s^{-1}. The length, perimeter and enclosed cross sectional end-areas of the pore used in this experiment were measured using the methods described in Section 2.3. Eqs. (A8) and (A11) were used to calculate the hydrodynamic length and radii of the pore. These calculated values were $L_h = 126.3 \pm 19$ μm, $a_h = 0.46 \pm 0.09$ μm and $b_h = 7.55 \pm 1.51$ μm. The errors in these dimensions are an estimate of the combined effects of errors in measurement by microscopy and possible changes in pore dimensions in the time between this measurement and the concentration measurements. In combination with the measured particle count rate $J = 6.65\ s^{-1}$ and the pressure $P = 981$ Pa, these values were used with Eq. (3) to calculate a particle concentration of $C = (1.05 \pm 0.69) \times 10^9\ ml^{-1}$. This calculated concentration is 86% larger than the concentration taken from the manufacturer's specifications ($5.68 \times 10^8\ ml^{-1}$). Possible sources of error that could account for this discrepancy include systematic errors in the determination of the concentration by the manufacturer, errors in measuring a_h and b_h, the not-perfectly conical shape of the pore, changes in the pore geometry between measurement of the pore dimensions and experiment, the loss of small events in current noise, particle aggregation and experimental errors in procedures such as pipetting. The largest errors are likely to be in the measured pore dimensions a, b and L, with the possibility of additional errors in the manufacturer-defined concentration. Errors made by the manufacturer in measuring the particle size would result in large errors when measuring the concentration using gravimetry. However, in this case the particles used were sized using NIST traceable methods, so these errors should be minimized. Errors in the measurement of the small pore size a will have a particularly large effect; in the case of a typical pore as used in this study, the small pore size is raised to the power of three in the equation for Q (see Eq. (A7)) (when $b = a$, the effect is even larger, as Q scales with a^4). An increase of only 23% in the small pore size (for example from 1 to 1.23 μm) would result in the 86% increase in concentration that we observe here. Given the elastic nature of the pore, it is not inconceivable that changes in the pore geometry may occur in the time between the measurement of the pore dimensions by electron microscopy and the experimental measurement of the particle count rate using SIOS. It is likely that this is the cause for the discrepancy between the measured and manufacturer-specified concentrations here. A similar discrepancy of 80% between the measured and manufacturer-defined concentration was found in an experiment using the same pore but a different particle (Th378, data not shown).

Both calibration methods have limitations; the calibration-free method requires labour-intensive microscopy to measure the pore dimensions, and subsequent changes in the pore geometry may have a large effect on errors in the measured concentration, while the external calibration method is susceptible to errors in the manufacturer-defined particle concentration. In all of the following experiments a sample of known concentration was used as a calibration to determine unknown concentrations.

The results shown here illustrate the ability of SIOS to measure in a model system of polystyrene particles, and results in the following sections detail the detection of viruses and bacteria. It should be noted that previous and current experiments have demonstrated that SIOS is able to detect a wide range of particle types. For example, using SIOS, bare, streptavidin-modified and streptavidin/DNA-modified organosilica particles have been distinguished (Roberts et al., 2010), size changes in gold nanoparticles have been measured after the attachment of nucleic acids (Low et al., in press), and lipid particles containing superparamagnetic iron oxide particles have been analyzed (Upadhyay et al., submitted for publication). Recent experiments (which are yet to be published) have also shown that DPPC liposomes can be readily sized using SIOS technology.

4.2. Viral concentration measurement

Baculoviruses are increasingly being developed as ecologically responsible alternatives to chemical insecticides (Szewczyk et al., 2006). The Baculovirus biopesticide product is actually an occlusion body (OB), a protein crystal in which the virus is embedded. The average diameter of OBs can range from 0.2 to 2 μm depending on the type of Baculovirus (Ackermann and Smirnoff, 1983); previous electron microscopy images (Lua et al., 2003) of limited numbers of Baculovirus OBs of the type measured here (derived from HaSNPV-infected *H. armigera* insect larvae) indicated an approximate diameter of ~1 μm. A major concern in developing a commercially viable manufacturing process is the accurate determination of OB concentration in the final formulation. The standard method of counting Baculovirus OBs uses a haemocytometer and a phase-contrast microscope (Chakraborty et al., 1996), but this methodology is time consuming, labour intensive and subjective, and hence it is highly desirable to develop an alternative OB enumeration methodology that is quick, robust, objective and accurate. The use of SIOS for the accurate measurement of total OB concentration is demonstrated here. Details of the virus purification and sample preparation are given in Section 2.2.

Before measuring the viral OB concentration, a size and concentration calibration was performed using Po920 particles, diluted to a concentration of $2.75 \times 10^7\ ml^{-1}$ in a Tris buffered KCl solution (diluted 2000 times from an original concentration of $5.5 \times 10^{10}\ ml^{-1}$). The size calibration was performed following the method described by Vogel et al. (2011). Data was then taken at applied pressures of 0 kPa, 0.3 kPa, 0.6 kPa and 0.9 kPa for the Baculovirus OB sample, which was diluted by a factor of 20 into Tris buffered KCl solution. The resulting size histogram for the Baculovirus OBs (shown in the inset in Fig. 2) gave a mean virus size of ~1.0 μm. This agrees with the available previous sizing data (Lua et al., 2003). It should be noted that the ability of SIOS to obtain size (Vogel et al., 2011) and concentration data from the same sample allows an extra confirmation of data reliability; one can use size data to make sure that one is measuring the

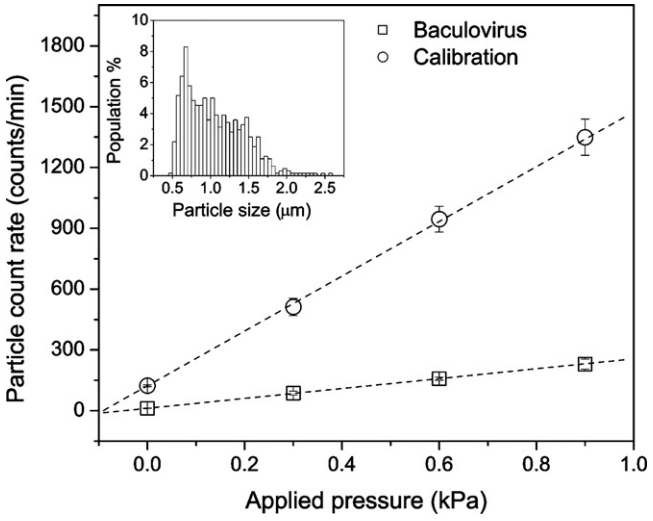

Fig. 2. Plot of particle count rate against applied pressure showing data for both HaSNPV Baculovirus OBs (square), and a calibration sample using Po920 particles (circle), with inset showing the particle size histogram for the Baculovirus OBs. The mean measured size for the Baculovirus OB was ~1.0 μm, and the viral concentration calculated using a comparison between the plotted gradients was $(9.9 \pm 0.8) \times 10^7\ ml^{-1}$.

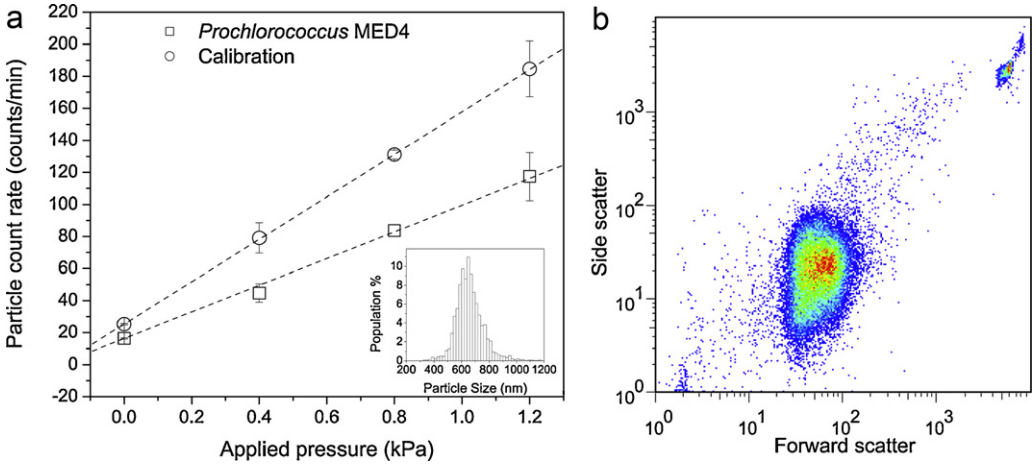

Fig. 3. (a) Plot of particle count rate against applied pressure showing data for both cyanobacterium *Prochlorococcus* MED4 bacteria (square), and the Th780 particle calibration sample (circle), with inset showing the particle size histogram for *Prochlorococcus* MED4. The mean measured size for *Prochlorococcus* MED4 was ~650 nm, and the bacterial concentration calculated using a comparison between the plotted gradients was $(6.0 \pm 0.4) \times 10^8$ ml^{-1}. (b) Flow cytometry plot showing side scatter against forward scatter for *Prochlorococcus* MED4. The concentration for *Prochlorococcus* as measured by flow cytometry was $(6.34 \pm 0.02) \times 10^8$ ml^{-1}.

concentration of the correct population. Fig. 2 shows plots of count rate (min^{-1}) against applied pressure for the calibration sample and the virus OB sample, with linear fits to the data, and error bars illustrating the repeatability of the measurements (the error bars show the standard deviation for measurements repeated in triplicate; the standard deviations were small, with values ranging from 4% to 11% of the mean count rate at each pressure). A concentration of $(9.9 \pm 0.8) \times 10^7$ ml^{-1} was calculated for the Baculovirus OB suspension. Measurements on the same sample in the same lab on a different date gave a very similar concentration (data not shown here). In order to check the validity of the Baculovirus OB concentration obtained using SIOS, a count was made using an improved Neubauer haemocytometer and a phase contrast microscope (Chakraborty et al., 1996). These counts were made in sextuplicate. The concentration obtained via microscopy was $(12.0 \pm 3.1) \times 10^7$ ml^{-1}, which agrees well with the concentration from SIOS. There is a 17% difference between the mean concentrations; the difference between these values is within the calculated experimental errors. The standard deviations for the repeated measurements have the same values as the calculated experimental errors (0.8×10^7 ml^{-1} and 3.1×10^7 ml^{-1} for SIOS and microscopy respectively). A *t*-test performed to compare the concentrations obtained using SIOS and counting by microscopy gave $P = 0.698$, showing that the results are similar and any differences are not significant. These results show that SIOS can be applied to accurately measure viral OB concentrations.

4.3. Bacterial concentration measurement

SIOS was also applied to measure concentrations of bodies in a different biological sample. The marine cyanobacterium *Prochlorococcus*, first described in 1988 (Chisholm et al., 1988), is the smallest (~600 nm) (Morel et al., 1993) and most abundant (Partensky et al., 1999) known photosynthetic organism. This bacterium has attracted interest as a model system for cross-scale biology (Coleman and Chisholm, 2007; Li, 2009) – while individual bacteria interact with their environment on length scales of nanometers to millimeters and timescales from seconds to hours, the larger ecosystem they contribute to may have inherent length and timescales as large as kilo- to megametres and years to decades (Li, 2009). The ubiquity, simplicity and genetic diversity of *Prochlorococcus* make it an ideal candidate to advance our understanding of biological diversity over these widely varying scales (Coleman and Chisholm, 2007). As part of this ongoing study, population numbers of *Prochlorococcus* are monitored over time and space via concentration measurements (Coleman and Chisholm, 2007). In order to demonstrate the efficacy of SIOS in measuring *Prochlorococcus* concentrations, axenic lab cultures of *Prochlorococcus* in seawater were analyzed and the results compared with flow cytometry data.

Before experiments the bacteria samples were diluted 1 in 100 into filtered seawater-based Pro99 medium. Prior to the analysis of the bacteria samples, a concentration calibration was carried out using Th780 particles suspended at a concentration of 9.50×10^6 ml^{-1} in seawater-based Pro99 (diluted from a stock concentration of 9.50×10^8 ml^{-1}). Data was then taken at applied pressures of 0 kPa, 0.4 kPa, 0.8 kPa and 1.2 kPa for the *Prochlorococcus* sample. The mean count rate per minute was calculated from repeated measurements. A size calibration (data shown in the inset of Fig. 3(a)) was performed using Th780 particles, following Vogel et al. (Vogel et al., 2011). A size range of between ~300 nm and ~1200 nm and a mean size of ~650 nm was found for *Prochlorococcus* MED4. Previous sizing of *Prochlorococcus* (giving a mean size of ~600 nm) agrees well with these values (Morel et al., 1993). Fig. 3(a) shows a plot of count rate (min^{-1}) against applied pressure with a linear fit to the data, with the measurement repeatability represented in the error bars (which show standard deviations calculated from measurements repeated in triplicate; the standard deviations were small, with values ranging from 2% to 13% of the mean count rate at each pressure). A concentration of $(6.0 \pm 0.4) \times 10^8$ ml^{-1} was calculated for the *Prochlorococcus* sample (measurements performed on the same sample in a different lab by a different user on a different date gave a very similar concentration – data not shown here). Flow cytometry performed on the same sample gave a concentration of $(6.34 \pm 0.02) \times 10^8$ ml^{-1}. (In the scatter plot shown in Fig. 3(b), each bacterium is represented by a dot, positioned according the forward (*x*-axis) and side (*y*-axis) scattered intensities detected for that bacterium. The density of dots in a region indicates the number density of bacteria of a certain size). The concentration obtained using SIOS agrees well with the value obtained using flow cytometry. There is a 6% difference between the mean concentrations; the difference between these values is within the calculated experimental error. The standard deviations for the repeated measurements have the same values as the calculated experimental errors (0.4×10^8 ml^{-1} and 0.02×10^8 ml^{-1} for SIOS and flow cytometry respectively). A *t*-test performed to compare the concentrations obtained using SIOS and counting by microscopy gave $P = 0.868$, showing that the results from the two methods are similar and any differences between

them are not significant. These results confirm the accuracy and validity of SIOS in measuring bacterial concentrations.

5. Conclusion

This work demonstrates the efficacy of SIOS in rapidly, accurately and directly measuring particle concentrations for a wide range of particle sizes in systems of both synthetic and biological nanoparticles. The change in event frequency (particle count rate) with applied pressure was used to quantitatively determine dispersion concentrations. Two calculation methods were demonstrated; a measurement of the pore dimensions allowed unknown concentrations to be calculated without the need for a calibration sample, and a calibration sample of known concentration was used to determine unknown concentrations. Experiments in a model system of polystyrene nanoparticles showed that, as expected from theory derived from the Hagen–Poiseuille equation, the particle count rate varies linearly with both pressure and suspension concentration. It was demonstrated that the determined concentration is independent of particle size or charge. The application of SIOS for measuring concentrations in biological samples was illustrated in samples of Baculovirus OBs (occlusion bodies) and the marine cyanobacterium *Prochlorococcus*. In both cases the concentration determined by SIOS agreed very closely with values obtained using conventional techniques – counting by microscopy in the case of Baculovirus OBs and flow cytometry for *Prochlorococcus*. These experiments covered a particle size range from ~200 nm to ~1 μm, which improves upon the size detection abilities of conventional techniques. The results shown here illustrate the ability of SIOS to characterize a diverse range of nanoparticle systems, and demonstrate its potential as a tool to be applied in virology, nanoparticle studies and measurements of bacterial concentrations.

Acknowledgements

We thank S.W. Chisholm for providing the facilities for the *Prochlorococcus* analyses, and Darby Kozak and Geoff Willmott for useful comments during the editing process.

Appendix A.

Particle concentrations are calculated using the expression

$$J = CQ \tag{A1}$$

where J is the particle count rate, C is the particle concentration and Q is the fluid flow rate (Deblois et al., 1977). Q is calculated using theory derived from the Hagen–Poiseuille equation (Tritton, 1988) for the pressure difference ΔP across a cylindrical pipe:

$$\Delta P = \frac{8\eta LQ}{\pi r^4} \tag{A2}$$

Here η is the fluid viscosity, L is the length of the pipe and r is the radius of the pipe. This expression must be modified to account for the near-conical geometry of the pores used in this study. If we consider a conical pipe with a small opening of radius a, a large opening of radius b and a length L, the radius a' at a given point x along the length of the pipe is

$$a' = \left(\frac{b-a}{L}\right)x + a \tag{A3}$$

From Eq. (A2)

$$dP = \frac{8\eta Q}{\pi(a')^4}dx \tag{A4}$$

Taking the derivative of Eq. (A3), rearranging for dx and substituting in Eq. (A4), we obtain the integral

$$P = \int_a^b \frac{8\eta Q}{\pi(a')^4}\frac{L}{b-a}da' \tag{A5}$$

Evaluating this integral and rearranging for Q gives the expression

$$Q = \frac{3\pi P}{8\eta L}\frac{b-a}{b^3-a^3}a^3b^3 \tag{A6}$$

In the limit $b \gg a$ this reduces to

$$Q = \frac{3\pi P}{8\eta L}a^3 b \tag{A7}$$

This expression ignores electroosmosis, while Eq. (A1) remains valid only if electrophoretic velocities are small compared to fluid velocities (Deblois et al., 1977). Previous work (Willmott et al., 2010) has shown that under conditions such as those used in this study (i.e. typical pore sizes and applied pressures) electrophoresis is dominated by the pressure-induced flow velocity, and the effects of electroosmosis are negligible, so these assumptions are valid.

Previous microscopy (Willmott et al., 2010) has shown that the pores used in SIOS are not perfectly round in cross section. For non-circular shapes the characteristic dimension is chosen to be the hydraulic diameter, which is given by (Fay, 1994)

$$D_h = 4\left(\frac{A}{p}\right) \tag{A8}$$

where A is the cross sectional area and p is the perimeter.

The pressure P in Eq. (A7) is also subject to a correction to account for end effects. The end correction for slow viscous flow (as applies in the experiments detailed here) in a long tube is given by (Weissberg, 1962)

$$P_{\text{edn}} = \frac{3\eta Q}{r^3} \tag{A9}$$

Applying this correction to the pressure as given in Eq. (A7), we obtain a total pressure of

$$P_{\text{tot}} = \frac{8\eta LQ}{3\pi a^3 b} + \frac{3\eta Q}{2a^3} + \frac{3\eta Q}{2b^3} \tag{A10}$$

Rearranging this equation allows an expression to be found for the hydrodynamic length L_h (Deblois et al., 1977), with the hydrodynamic radii a_h and b_h as calculated from Eq. (A8) used in the place of the geometric radii:

$$L_h = L + \frac{9\pi}{16}b_h + \frac{9\pi}{16}\frac{a_h^3}{b_h^2} \tag{A11}$$

Incorporating the hydrodynamic length and radii into Eq. (A6) and substituting for Q in Eq. (A1) gives the full expression for the theoretical particle concentration:

$$C = J\left(\frac{3\pi P}{8\eta L_h}\frac{b_h - a_h}{b_h^3 - a_h^3}a_h^3 b_h^3\right)^{-1} \tag{A12}$$

References

Ackermann, H.W., Smirnoff, W., 1983. Journal of Invertebrate Pathology 41 (3), 269–280.
Alberts, B., Bray, D., Lewis, J., Raff, M., Roberts, K., Watson, J., 1994. Molecular Biology of the Cell. Garland, New York.
Bayley, H., Martin, C.R., 2000. Chemical Reviews 100 (7), 2575–2594.
Bondoc-Jr, L., Fitzpatrick, S., 1998. Journal of Industrial Microbiology and Biotechnology 20 (6), 317–322.
Brannon-Peppas, L., Blanchette, J.O., 2004. Advanced Drug Delivery Reviews 56 (11), 1649–1659.
Campos, S.K., Barry, M.A., 2007. Current Gene Therapy 7 (3), 189–204.
Chakraborty, S., Greenfield, P., Reid, S., 1996. Cytotechnology 22 (1), 217–224.

Chisholm, S.W., Olson, R.J., Zettler, E.R., Goericke, R., Waterbury, J.B., Welschmeyer, N.A., 1988. Nature 334 (6180), 340–343.
Chithrani, B.D., Ghazani, A.A., Chan, W.C.W., 2006. Nano Letters 6 (4), 662–668.
Cohen-Sela, E., Rosenzweig, O., Gao, J., Epstein, H., Gati, I., Reich, R., Danenberg, H.D., Golomb, G., 2006. Journal of Controlled Release 113 (1), 23–30.
Coleman, M.L., Chisholm, S.W., 2007. Trends in Microbiology 15 (9), 398–407.
Colson, Y.L., Liu, R., Southard, E.B., Schulz, M.D., Wade, J.E., Griset, A.P., Zubris, K.A.V., Padera, R.F., Grinstaff, M.W., 2011. Biomaterials 32 (3), 832–840.
Cuenca, A.G., Jiang, H.B., Hochwald, S.N., Delano, M., Cance, W.G., Grobmyer, S.R., 2006. Cancer 107 (3), 459–466.
Cui, Z.R., Lockman, P.R., Atwood, C.S., Hsu, C.H., Gupte, A., Allen, D.D., Mumper, R.J., 2005. European Journal of Pharmaceutics and Biopharmaceutics 59 (2), 263–272.
Deblois, R.W., Bean, C.P., 1970. Review of Scientific Instruments 41 (7), 909–916.
Deblois, R.W., Bean, C.P., Wesley, R.K.A., 1977. Journal of Colloid and Interface Science 61 (2), 323–335.
Deblois, R.W., Wesley, R.K., 1977. Journal of Virology 23 (2), 227–233.
Fay, J., 1994. Introduction to Fluid Mechanics, 2nd ed. The MIT Press.
Ferrari, M., 2008. Nature Nanotechnology 3 (3), 131–132.
Fraikin, J.L., Teesalu, T., McKenney, C.M., Ruoslahti, E., Cleland, A.N., 2011. Nature Nanotechnology 6 (5), 308–313.
Ito, T., Sun, L., Henriquez, R.R., Crooks, R.M., 2004. Accounts of Chemical Research 37 (12), 937–945.
Jiang, W., Kim, B.Y.S., Rutka, J.T., Chan, W.C.W., 2008. Nature Nanotechnology 3 (3), 145–150.
Jin, S., Ye, K.M., 2007. Biotechnology Progress 23 (1), 32–41.
Johansson, M.E., Uhnoo, I., Kidd, A.H., Madeley, C.R., Wadell, G., 1980. Journal of Clinical Microbiology 12 (1), 95–100.
Joshi, P., Mathew, T., Petrossian, L., Prasad, S., Goryll, M., Spanias, A., Thornton, T., 2009. ASME 2009 International Mechanical Engineering Congress and Exposition , ASME, Lake Buena Vista, Florida, USA.
Kozak, D., Anderson, W., Vogel, R., Trau, M., 2011. NanoToday 6 (5), 531–545, doi:10.1016/j.nantod.2011.08.012.
Li, W.K.W., 2009. Aquatic Microbial Ecology 57 (3), 239–251.
Low, M., Yu, S., Han, M.Y., Su, X., 2011. Australian Journal of Chemistry, in press. doi:10.1071/CH11200.
Lua, L.H.L., Nielsen, L.K., Reid, S., 2003. Biological Control 26 (1), 57–67.
Ma, L., Bluyssen, H.A.R., De Raeymaeker, M., Laurysens, V., van der Beek, N., Pavliska, H., van Zonneveld, A.-J., Tomme, P., van Es, H.H.G., 2001. Journal of Virological Methods 93 (1–2), 181–188.
Maizel, J.V., White, D.O., Scharff, M.D., 1968. Virology 36 (1), 115–125.
Moore, L.R., Post, A.F., Rocap, G., Chisholm, S.W., 2002. Limnology and Oceanography 47 (4), 989–996.
Morel, A., Ahn, Y., Partensky, F., Vaulot, D., Claustre, H., 1993. Journal of Marine Research 51 (3), 617–649.
Mukherjee, P., Bhattacharya, R., Bone, N., Lee, Y., Patra, C., Wang, S., Lu, L., Secreto, C., Banerjee, P., Yaszemski, M., 2007. Journal of Nanobiotechnology 5 (4).
Nienhuis, A.W., 2008. Blood 111 (9), 4431–4444.
Oh, S., Kim, C., Cha, H., Pal, U., Kang, Y., 2009. Advanced Materials 21 (48), 4987–4991.
Park, L.S., Park, J.W., Choi, H.Y., Han, Y.S., Kwon, Y., Choi, H.S., 2006. Current Applied Physics 6 (4), 644–648.
Partensky, F., Hess, W., Vaulot, D., 1999. Microbiology and Molecular Biology Reviews 63 (1), 106.
Roberts, G.S., Kozak, D., Anderson, W., Broom, M.F., Vogel, R., Trau, M., 2010. Small 6 (23), 2653–2658.
Russel, W., Saville, D., Schowalter, W., 1992. Colloidal Dispersions. Cambridge University Press.
Saleh, O.A., Sohn, L.L., 2001. Review of Scientific Instruments 72 (12), 4449–4451.
Shapiro, H.M., 2003. Practical Flow Cytometry, 4th ed. Wiley-Blackwell.
Sowerby, S.J., Broom, M.F., Petersen, G.B., 2007. Sensors and Actuators B: Chemical 123 (1), 325–330.
Szewczyk, B., Hoyos-Carvajal, L., Paluszek, M., Skrzecz, W., de Souza, M.L., 2006. Biotechnology Advances 24 (2), 143–160.
Tanaka, T., Decuzzi, P., Cristofanilli, M., Sakamoto, J.H., Tasciotti, E., Robertson, F.M., Ferrari, M., 2009. Biomedical Microdevices 11 (1), 49–63.
Tritton, D., 1988. Physical Fluid Dynamics, 2nd ed. Oxford University Press, Oxford.
Upadhyay, D., Scalia, S., Wheate, N., Vogel, R., Salama, R.O., Young, P.M., Traini, D., Chrzanowski, W., submitted for publication.
Vogel, R., Willmott, G., Kozak, D., Roberts, G.S., Anderson, W., Groenewegen, L., Glossop, B., Barnett, A., Turner, A., Trau, M., 2011. Analytical Chemistry 83 (9), 3499–3506.
Weissberg, H., 1962. Physics of Fluids 5, 1033.
Westedt, U., Barbu-Tudoran, L., Schaper, A.K., Kalinowski, M., Alfke, H., Kissel, T., 2004. European Journal of Pharmaceutics and Biopharmaceutics 58 (1), 161–168.
Willmott, G.R., Moore, P.W., 2008. Nanotechnology 19 (47).
Willmott, G.R., Vogel, R., Yu, S.S.C., Groenewegen, L.G., Roberts, G.S., Kozak, D., Anderson, W., Trau, M., 2010. Journal of Physics: Condensed Matter 22 (45).